

Electric field and exciton structure in CdSe nanocrystals

E. M. Fernández-Proupin and C. Trallero-Giner

IM RE-Facultad de Física, Universidad de La Habana, Vedado 10400, La Habana, Cuba

(Dated: April 14, 2024)

Quantum Stark effect in semiconductor nanocrystals is theoretically investigated, using the effective mass formalism within a 4 × 4 Baldereschi-Lipari Hamiltonian model for the hole states. General expressions are reported for the hole eigenfunctions at zero electric field. Electron and hole single particle energies as functions of the electric field (E_{QD}) are reported. Stark shift and binding energy of the excitonic levels are obtained by full diagonalization of the correlated electron-hole Hamiltonian in presence of the external field. Particularly, the structure of the lower excitonic states and their symmetry properties in CdSe nanocrystals are studied. It is found that the dependence of the exciton binding energy upon the applied field is strongly reduced for small quantum dot radius. Optical selection rules for absorption and luminescence are obtained. The electric-field induced quenching of the optical spectra as a function of E_{QD} is studied in terms of the exciton dipole matrix element. It is predicted that photoluminescence spectra present anomalous field dependence of the emission lines. These results agree in magnitude with experimental observation and with the main features of photoluminescence experiments in nanostructures.

PACS numbers: 73.21.La, 73.22.-f, 78.67.-n

Keywords: quantum dots, nanocrystals, Stark effect, quenching

I. INTRODUCTION

Semiconductor nanostructures under longitudinal electric field produce pronounced effects on optical properties.^{1,2,3,4,5,6,7} It has been shown that the field induces a red shift of the exciton peaks in the photoluminescence and electro-optical spectra. The shift of the excitonic peaks to lower energy with the increasing electric fields is known as quantum Stark effect, while the reduction of the overlapping between the electron-hole pair wave function by the field is related to quenching of the fundamental transition in the luminescence spectrum. Zero dimensional systems as colloidal semiconductor quantum dots (QDs) under electric fields are appropriate candidates for several device applications, including optical computing and fiber-optical communication (see Ref. 8 and references therein). Also, the micro-photoluminescence spectroscopic technique in single spherical QDs has allowed to study fundamental issues of the excitonic states.⁹

The electro-optical properties, the Stark shift, and the dependence of the peak intensity in the optical spectra upon the applied field should depend strongly upon the details of the band structure. This was demonstrated for quantum wells in the 80's.^{10,11,12} It is interesting to investigate the analogous effects in QD, as the three-dimensional confinement causes properties that are beyond the naive enhancement of the effects observed in quantum wells. For example, in QDs the band dispersion no longer exists, the energy spectrum is totally discrete and depends qualitatively upon the dot geometry. Moreover, the high surface to volume ratio originates effects that are intrinsic to QDs. Perhaps, the most spectacular finding up to date is the discovery of high luminescence in porous Si,¹³ where QDs are believed to play an important role.¹⁴ Other striking effects can be found in the

dark magneto-exciton luminescence,¹⁵ and the blinking and spectral shifting of single QD luminescence under external electric fields.⁸

Calculations of the quantum Stark effect in spherical QDs in the strong confinement regime have been performed in the framework of the parabolic model.^{16,17} The simple parabolic model was able to provide a relative good picture for the description of the electronic states in the conduction band. This approximation breaks down for the calculation of the hole levels due to the fourfold degeneracy and the admixture of the light and heavy-hole bands present in the II-VI and II-III compounds with zinc-blende lattice structure. A reliable description of the energy band dispersion is ruled by the Baldereschi-Lipari Hamiltonian.¹⁸ Within this approach, calculations of the influence of an external electric field E_{QD} were done in Ref. 19. However, this calculation presents several limitations (for a detailed discussion see Ref. 20). As it is well known, the dependence of the interband optical transitions upon the light frequency (absorbed or emitted) reflects the structure of the conduction and valence bands.

In this paper we study the excitonic Stark effect of spherical QDs taking into account the valence band admixture using the Baldereschi-Lipari Hamiltonian¹⁸. Supported by a rigorous treatment of the exciton wavefunctions, we have obtained the interband dipole matrix elements taking into account the fundamental symmetry properties of the QD. From the dipole matrix elements we have obtained the optical selection rules that allow the identification of the exciton levels observed in absorption and luminescence experiments. We present numerical calculations that reveal the combined effects of band admixture, Coulomb interaction, QD size and electric field intensity.

In Sec. II we examine the energy dependence upon E_{QD} for the electrons and holes in CdSe QDs. Explicit

analytical solutions for the hole levels at $E_{QD} = 0$ are derived. The influence of Coulomb correlation and valence band coupling on the quantum Stark effect is analyzed in Sec. III. Section IV is devoted to study the electric-field induced optical properties. The main results of the paper are summarized in Sec. V.

II. SINGLE PARTICLE STATES

In the effective mass approximation, the Stark effect on the electronic states at the bottom of the conduction band can be represented by products of the $\ell=2$ Bloch functions $h_{rj\ell=2;s_z i}$ (with s_z being the conduction band-edge angular momentum and $s_z = \pm 1/2$) times envelope functions. The latter ones are obtained from the effective mass Hamiltonian with a uniform electric field $\mathcal{E}_{QD} r \cos \theta$. Here, e is the electron charge and E_{QD} is the electric field intensity inside the nanocrystal. At zero electric field, the envelope functions take the form $R_{n1}(r)Y_{1\ell_z}(\theta; \phi)$. $R_{n1}(r)$ are the radial wave functions,²¹ and $Y_{1\ell_z}(\theta; \phi)$ are the spherical harmonics.²² These states are in the $\ell=1$ coupling scheme and have well defined values of the squared orbital and spin angular momenta. Instead, we will use the $\ell=2$ coupling scheme, where the states have well defined total ($f = l + s$) angular momentum projection $\sim f_z$ and square value $\sim f(f+1)$; that is

$$\begin{aligned} h_{rj\ell=2;s_z i} = & \sum_{\ell_z} (1/2 \ell_z s_z | f f_z) R_{n1}(r) Y_{1\ell_z}(\theta; \phi) h_{rj\ell=2;s_z i}; \quad (1) \\ & \ell_z, s_z \end{aligned}$$

where $(1/2 \ell_z s_z | f f_z)$ are the Clebsch-Gordan coefficients, $f = \ell_z + s_z$, and $j = \ell = 2$, $f = 1 + 1 = 2$.²³ If the hole states in the valence bands are described by an spherical 4×4 $k \cdot p$ Hamiltonian, the $\ell=2$ coupling scheme for the electron wave function is more convenient to build up the excitonic states in a spherical QD. The hole and electron states present the same symmetry properties, allowing to use all inherent properties of the Clebsch-Gordan coefficients.²⁴

Since the $s_z = \pm 1/2$ bands are uncoupled, the states described by Eq. (1) have energies $E_{n,1}^e$ that are independent of the quantum numbers $f; f_z$. In the simulation of the real electronic states, the confinement potential is chosen as a spherical box with an effective radius R_{ef} , which is greater than the structural nanocrystal radius R . This effective radius is introduced in order to take into account, approximately, the penetration of the electron wave function in the surrounding medium. In our calculations, we determine R_{ef} from the condition that the energy of the $1s$ state $E_{1,0} = \sim \frac{1}{2} \frac{\hbar^2}{2m_e R_{ef}^2}$ be equal to the energy calculated for a spherical well with depth $V_e = 600$ meV.²⁵

The electron states under external electric fields are found by numerical diagonalization of H_e in the basis provided by (1). The matrix elements of the Stark term are provided in the Appendix.

TABLE I: Parameters used in the calculations.

Parameter	CdSe
E_g (eV)	1.841 ²⁶
$m_e = m_0$	0.13 ²⁵
1	1.66 ²⁵
2	0.41 ²⁵
$2m_0 P^2$ (eV) ^a	20 ²⁷
	9.53 ²⁸
V_e (eV)	0.6 ²⁵
V_h (eV)	1 ²⁵

$$^a P = \frac{1}{2} \hbar s_j p_x j x i = m_0.$$

For the hole states in the bottom of the valence band we use the well known Baldeschwi-Lipari Hamiltonian^{18,29,30} in presence of a constant electric field, that is

$$\begin{aligned} H_h = & \frac{1}{2m_0} p^2 - \frac{\hbar}{9} P^{(2)} J^{(2)} + V_h(r) \mathcal{E}_{QD} r \cos \theta; \quad (2) \end{aligned}$$

$V_h(r)$ being the confinement potential for the valence band, $P^{(2)}$ and $J^{(2)}$ are spherical tensors of rank 2 built from linear and angular momentum operators, $P = 2/3$, and J_2 and J_1 are the Luttinger parameters of CdSe in the spherical approximation $J_2 = 3$. The hole eigenfunctions at zero electric field can be cast as

$$\begin{aligned} h_{rj\ell=2;s_z i} = & \sum_{K} \sum_{\ell_z} (K \frac{1}{2} \ell_z J_z | f f_z) R_{N,K}^{(F)}(r) Y_{K \ell_z}(\theta; \phi) h_{rj\ell=2;s_z i}; \quad (3) \end{aligned}$$

where $h_{rj\ell=2;s_z i}$ are the hole Bloch functions of the $\ell=2$ valence band with band-edge angular momentum $J = 3/2$. The hole Bloch functions are related with the valence electron Bloch functions $\overline{h_{rj\ell=2;s_z i}}$ by the rule $j J_z i = (-1)^{J-J_z} \overline{j J_z i}$ (derived from the time-reversal operation). Our Bloch functions $\beta=2; J_z i$ have the following phase convention: $\beta=2; J_z=3/2 i = (-1)^{J-J_z} (i=2) (X \pm iY) j i$, and $\beta=2; J_z=1/2 i = (-1)^{J-J_z} (i=6) (2Z \pm iY) j i$. The phase factors of the above Bloch functions are implicit in the optical dipole matrix elements.

For $F = 1/2$, according to the rule of the addition of two angular momenta, $J = 3/2 + F = L + 3/2$, the states defined in Eq. (3) reduce to two uncoupled states $L = 1$ ($K = 1$) and $L = 2$ ($K = 2$) which correspond to $P_{1=2}$ and $D_{1=2}$ states with radial wave functions $R_{N,\ell}^{(1=2)}$ ($L = 1; 2$). In this case the eigenfunctions $R_{N,\ell}^{(1=2)}$ fulfill two independent radial effective mass equations with light hole effective mass $m_{lh} = m_0 = (1 + 2/3)$.

For $F = 3/2$, the radial wave functions $R_{N,K}^{(F)}(r)$ are solutions of the coupled differential equations^{29,30}

$$\begin{aligned}
& (1 + C_1) \frac{d^2}{dr^2} + \frac{2}{r} \frac{d}{dr} - \frac{L(L+1)}{r^2} + W(r; E) \quad C_2 \frac{d^2}{dr^2} + \frac{2L+5}{r} \frac{d}{dr} + \frac{(L+1)(L+3)}{r^2} \\
& C_2 \frac{d^2}{dr^2} + \frac{2L+1}{r} \frac{d}{dr} + \frac{L(L+2)}{r^2} \quad (1 + C_3) \frac{d^2}{dr^2} + \frac{2}{r} \frac{d}{dr} - \frac{(L+2)(L+3)}{r^2} + W(r; E)
\end{aligned}
\tag{4}$$

where $W(r; E) = 2m_0 [V_h(r) - E] = -\frac{1}{2} R^2$.

The coefficients C_1 , C_2 and C_3 are reported for several states in Refs. 18 and 29. Following the argument of Baldereschi and Lipari, we have obtained the general expressions

$$C_1(L; F) = \frac{P}{5} \frac{(L+1)^{3=2+L+F} \frac{L}{3=2} \frac{L}{3=2} \frac{2}{F}}{\frac{2L(2L+1)(2L+2)}{(2L+3)(2L-1)}}; \tag{5a}$$

$$C_2(L; F) = \frac{P}{30} \frac{(L+1)^{3=2+L+F} \frac{L+2}{3=2} \frac{L}{3=2} \frac{2}{F}}{\frac{(L+1)(L+2)}{2L+3}}; \tag{5b}$$

$$C_3(L; F) = C_1(L+2; F) = C_1(L; F); \tag{5c}$$

The result $C_3 = C_1$ has been verified numerically. We also found numerically that $C_1^2 + C_2^2 = 1$ and $C_2 = > 0$.

In the case of abrupt infinite confinement potential, the solutions of equations (4) are

$$R_{N;L}^{(F)}(r) = A \frac{j_L(kr=R)}{j_L(k)} \frac{j_L(kr=R)}{j_L(k)}; \tag{6a}$$

$$R_{N;L+2}^{(F)}(r) = A \frac{C_1=C_2 + \frac{P}{(C_1=C_2)^2 + 1} \frac{j_{L+2}(kr=R)}{j_{L+2}(k)}}{C_1=C_2 + \frac{P}{(C_1=C_2)^2 + 1}}; \tag{6b}$$

where $\gamma = m_{lh} = m_{hh}$ ($m_{hh} = m_0 = \frac{1}{2} \frac{m_0}{m_{hh}}$) is the heavy hole mass. The parameter k fulfills the transcendental equation,

$$\frac{j_L(k)}{j_{L+2}(k)} \frac{j_L(k)}{j_{L+2}(k)} \frac{C_1=C_2 + \frac{P}{(C_1=C_2)^2 + 1}}{C_1=C_2 + \frac{P}{(C_1=C_2)^2 + 1}} = 1; \tag{7}$$

and A is a normalization constant, such that

$$\int_0^R R_{N;L}^{(F)}(r)^2 + R_{N;L+2}^{(F)}(r)^2 r^2 dr = 1; \tag{8}$$

The hole energies are equal to $E_h = -\frac{1}{2} k^2 = -2m_{hh} R^2$.

As in the case of the conduction band levels, the hole states under external electric field are found by numerical diagonalization of the Hamiltonian H_h in the basis provided by Eq. (3). The matrix element of the Stark term are provided in the Appendix.

Figure 1 shows the energy levels of electrons and holes as functions of the electric field intensity. The energies

are in units of $E_0 = \frac{1}{2} \hbar^2 R^2$ ($i = e, h$), and the electric field intensity is in units of $E_0 = \frac{1}{2} \hbar R$. In this figure, R for the electrons is the effective radius above introduced. The states at zero field are indicated by the usual spectroscopy notation $N A$, with $A = S; P; D; \dots (s; p; d; \dots)$ for the $L = 0; 1; 2; \dots (l = 0; 1; 2; \dots)$ hole (electron) states. In the case of the hole energies, the quantum number F is indicated by a sub-index, that is, $N A_F$: In the figure the values of j_L and j_{L+2} for each state are indicated and, as it can be seen, at non-zero electric field the j_L and the j_{L+2} degeneracy remains. For the electrons, due to the absence of Bloch-envelope (spin-orbit-like) coupling, there is an additional degeneracy. Thus, the electron energy levels only depend upon the modulus of the angular momentum projection j_L , being degenerate in the spin projection. The results for the electrons here shown reproduce those of Ref. 16. The light hole energies, which correspond to $F = 1=2$, are higher and are not included in Fig. 1.

The hole Hamiltonian (2) does not include band warping terms that arise from the cubic symmetry of the nanocrystal lattice. The cubic corrections are proportional to the cubic coupling parameter³¹ $\gamma_3 = \frac{1}{3} \gamma_2 = 1$. The Luttinger parameter γ_3 has not been determined for CdSe, but it has been estimated as 0.53²⁵ assuming that the ratio $\gamma_3 = \gamma_2$ is equal in CdTe and CdSe. Hence, a value $\gamma_3 = 0.066$ is obtained, which is one order of

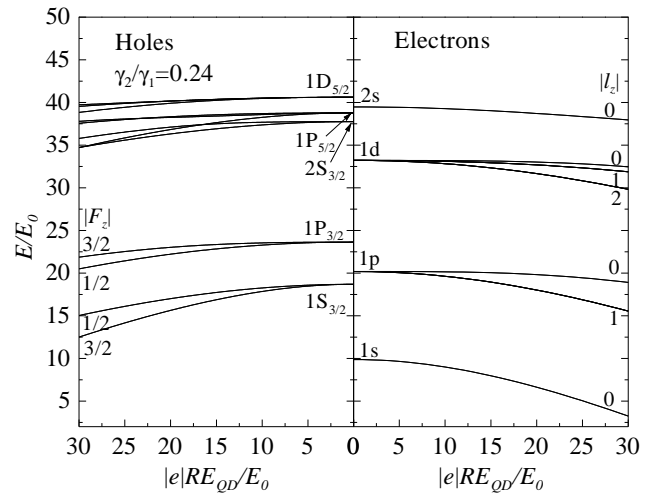


FIG. 1: Single particle energies vs. electric field intensity. Note that $E_0 = \frac{1}{2} \hbar^2 R^2$ depends upon the quasiparticle effective mass.

magnitude smaller than the spherical coupling parameter. Therefore, the cubic corrections can be included using perturbation theory. For zinc-blende semiconductors, parity-breaking terms exist, in principle. However, this effect seems to be smaller and the optical properties of acceptor levels have been explained without considering them.³¹ For zero electric field, the hole states $P_{1=2}$ and $D_{1=2}$ belong to the irreducible representations Γ_6 and Γ_7 of the point group T_d , respectively, while $S_{3=2}$ and $P_{3=2}$ states belong to the irreducible representation Γ_8 . Hence, their energies do not split and the selection rules are not modified for these states. However, the energy values shift in second order of \mathcal{E} , unless coupled quasidegenerate states are present.³¹ This is the case of the coupled states $2S_{3=2} - 1D_{5=2}$, where the splitting is first order in \mathcal{E} . For each $F > 3=2$, the eigenstates of the cubic Hamiltonian are formed of linear combinations of states with different F_z . These linear combinations transform according to the irreducible representations of T_d that are compatible with the representation D_F of the 3-dimensional rotation group $O(3)$. Hence, the analyzed levels split proportionally to \mathcal{E} in several levels, according to the compatibility tables of groups T_d and $O(3)$.³² The optical selection rules are relaxed for these states and additional transitions should appear with low intensity. The effects of the cubic anisotropy has been studied numerically for CdSe QDs using the Effective Bond Orbital Method (EBOM),²⁵ which implicitly takes into account the lack of inversion symmetry. It was shown that the spherical approximation is very good, specially for large nanocrystals.

III. EXCITON STATES

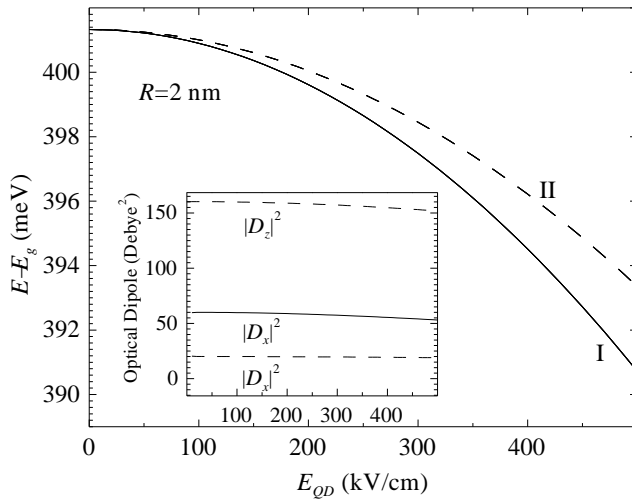


FIG. 2: Energy levels vs electric field of the lower excitonic states of a CdSe nanocrystal 2 nm in radius. The inset shows the allowed optical dipole matrix elements squared (see Sec. IV). By symmetry the components D_y and D_x are equal.

The exciton Hamiltonian can be written as the sum of the electron and hole Hamiltonians plus the screened Coulomb interaction $V_{eh} = -e^2 / (\epsilon_e \epsilon_h r_{eh})$, being the dielectric constant. Excitonic states, can be obtained using an expansion in a basis of electron-hole pair wave functions with well defined total angular momentum square $\sim^2 M(M+1)$ and projection $\sim M_z$

$$\begin{aligned} |j_i\rangle &= \sum_{N, L, F, F_z} C_{jN, L, F, F_z; M, M_z} |N, L, F, F_z; M, M_z\rangle; \quad (9) \\ &= f_{N, N_z} |j, L, F, F_z; M, M_z\rangle \end{aligned}$$

where

$$\begin{aligned} &\sum_{N, L, F, F_z} C_{jN, L, F, F_z; M, M_z} |N, L, F, F_z; M, M_z\rangle \\ &= \sum_{F_z, F_z'} (f_{F_z, F_z'} |F, F_z; M, M_z\rangle) \sum_{N, L, F, F_z} C_{jN, L, F, F_z; M, M_z} |N, L, F, F_z; M, M_z\rangle; \quad (10) \end{aligned}$$

It is important to remark that in Eqs. (9) and (10) it is implicit the condition for the addition of two angular momenta for electrons and holes $j_1 = 2, j_2 = 1, f = 1=2$ and $j_1 = 3=2, j_2 = L, F = 3=2$, respectively. The matrix elements of the Coulomb interaction in the basis (9) are reported in Ref. 33. The matrix elements of the Stark term are provided in the Appendix.

As the electric field is chosen along the Z-axis, the exciton angular momentum Z-projection is a constant of motion and the Hamiltonian can be diagonalized independently in different M_z -subspaces. We have built the M_z -subspaces using as basis all the possible electron-holes states (10) that fulfill the condition $2m_e R^2 E = \sim^2 90$ ($i = e; hh$). With these criteria the dimensions of the diagonalized matrices are 532, 502, and 415 for $M_z = 0, 1$, and 2, respectively.

Figure 2 shows the structure of the lower exciton energy level as a function of the applied electric field E_{QD} in a CdSe nanocrystal 2 nm in radius. The lower exciton at zero electric field is 8-fold degenerate: 3 states with $M = 1$ and 5 states with $M = 2$. All these states are originated from the $1s-1S_{3=2}$ electron-hole pairs. The electric field splits this level in two quartets: the lower one (I) belongs to states with $M_z = -1; 2$ while the higher level (II) in Fig. 2 corresponds to exciton wave function with $M_z = 0; 0; 1$. The inset in Fig. 2 displays the matrix elements of the dipole operator, which determine the optical properties and will be discussed in the next section. Table II illustrates the fraction contribution, $|C_{M, M_z}|^2$; of the dominant M -components in the expansion (9) to the excitonic levels I and II at $E_{QD} = 500$ kV/cm. It is worth to note that the states with $M_z = -1$ are derived from the $M = 1$ and 2 zero-field exciton wave functions, which are coupled by the electric field through remote states. The following group of exciton levels arises from the $1s-1P_{3=2}$ electron-hole pairs, with a splitting pattern similar to that of the lower level. In general, all the $M_z = 0$ levels are doubly degenerate. It is important to remark that the above description is valid for larger nanocrystals in the strong confinement regime.

The dependence of the binding energy upon E_{QD} , corresponding to the I and II exciton levels are shown in

Fig. 3 for several nanocrystal radii.

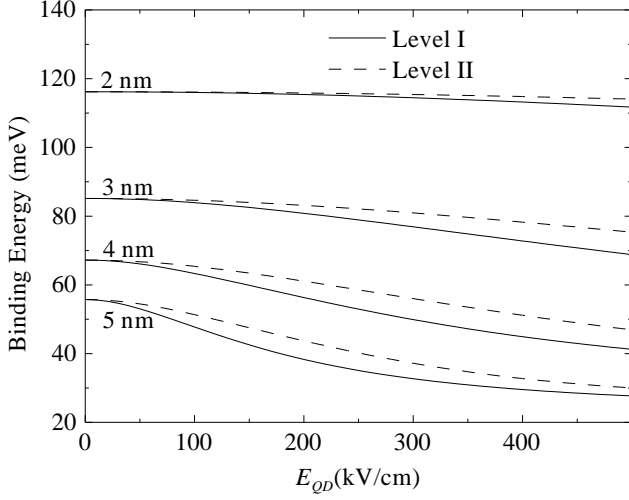
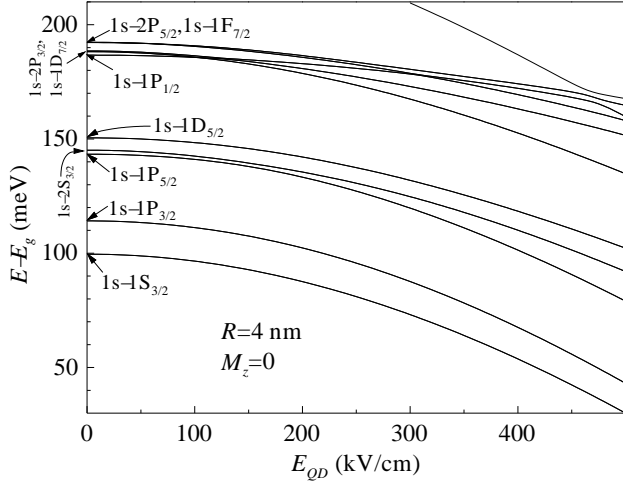


FIG. 3: Exciton binding energy versus electric field for the levels I and II shown in Fig. 2 for four QD radius (2,3,4, and 5 nm).

FIG. 4: Exciton energies with quantum number $M_z = 0$ vs electric field intensity for a CdSe nanocrystal 4 nm in radius.

The energy levels with $M_z = 0$, up to 100 meV above the lowest exciton, are plotted in Fig. 4. The states are labeled by the pure electron-hole pair contribution at zero field. Notably, no anti-crossing behavior is observed in levels $1s-1S_{3/2}$ and $1s-1P_{3/2}$, and there is a weak anti-crossing between $1s-1D_{5/2}$ and $1s-2S_{3/2}$ in the region 100–150 kV/cm. The anticrossings should not be altered by the effect of the cubic terms in the hole Hamiltonian, although the absolute values will change.

TABLE II: Fraction of the dominant M -component $\langle \mathcal{J}_M(M_z) \rangle^2$ to the expansion (9) for the lower excitonic states I and II shown in Fig. 2 at the electric field intensity $E_{QD} = 500$ kV/cm.

Level	I		II	
$E - E_g$	390.7 meV		393.4 meV	
	$\langle \mathcal{J}_M(M_z) \rangle^2$ -fraction		$\langle \mathcal{J}_M(M_z) \rangle^2$ -fraction	
$M - nM_z$	(2)	(1)	0	0 (1)
0	0	0	0	0.01 0
1	0	0.74	0.02	0.96 0.25
2	0.99	0.25	0.96	0.03 0.74
3	0.01	0	0.02	0 0.01

IV. FIELD INDUCED OPTICAL PROPERTIES

In the optical experiments the intensity of the absorbed or emitted light is proportional to the exciton oscillator strength (squared absolute values of the dipole matrix element between the ground and excited states of the quantum dot). The field will modify the electron and hole wave functions which determine the exciton oscillator strength. As the field delocalizes the electron and holes in opposite directions, in principle the allowed excitonic transitions should decrease as the applied electric field increases. This is related to the quenching of the luminescence spectra.^{34,35} Moreover, the field breaks the inner spherical symmetry of the dot and forbidden excitonic transitions should appear in the optical spectra for large electric fields.

The optical matrix element of the dipole operator for the exciton (9) is given by

$$D_{\mu G} = \sum_{\mathbf{r}} \langle \mathbf{r} | \hat{\mathbf{D}}_{\mu} | G \rangle = \sum_{\mathbf{r}} \langle \mathbf{r} | \hat{\mathbf{D}}_{\mu} | G \rangle; \quad (11)$$

$$= \sum_{\mathbf{r}} \langle \mathbf{r} | \hat{\mathbf{D}}_{\mu} | G \rangle = \sum_{\mathbf{r}} \langle \mathbf{r} | \hat{\mathbf{D}}_{\mu} | G \rangle$$

where G represents the nanocrystal ground state and $D_{\mu G} = \langle \mathbf{r} | \hat{\mathbf{D}}_{\mu} | G \rangle = \langle \mathbf{r} | \hat{\mathbf{D}}_{\mu} | G \rangle$ are the dipole matrix elements for the uncorrelated electron-hole pairs (Eq. 10), which are given in Ref. 33. These dipole matrix elements are different from zero only for $M = 1$ and are proportional to $\hat{\mathbf{e}}_{M_z}$, where $\hat{\mathbf{e}}_{M_z=0} = \hat{\mathbf{e}}_z$ and $\hat{\mathbf{e}}_{M_z=1} = (\hat{\mathbf{e}}_x \pm i\hat{\mathbf{e}}_y)/\sqrt{2}$ are the unit vectors in the spherical representation. This accounts for the optical selection rules in the dipole approximation: the only optically active electron-hole pairs have $M_z = 0$; 1 , and $M = 1$. According to the results of Table I, the exciton level I in Fig. 2 is optically active for light polarized (with electric polarization vector \mathbf{e}_1) along $\hat{\mathbf{e}}_x$ or equivalently $\mathbf{e}_1 \parallel \hat{\mathbf{e}}_{M_z=1}$, while the state II is allowed for $\mathbf{e}_1 \parallel \hat{\mathbf{e}}_z$ or $\mathbf{e}_1 \parallel \hat{\mathbf{e}}_{M_z=0}$. The corresponding squares of the dipole matrix elements $\langle \mathcal{J}_z \rangle^2 = \langle \mathcal{D}_{\mu G} \rangle^2$ and $\langle \mathcal{J}_x \rangle^2 = \langle \mathcal{D}_{\mu G} \rangle^2$ for the states I and II are shown in the inset of Fig. 2. Note that at zero electric field the sum of $\langle \mathcal{J}_x \rangle^2$ over all $M_z = 1$ states equals to $\langle \mathcal{J}_z \rangle^2$, as required by the spherical symmetry of our Hamiltonian.

Figure 5 shows the dependence of $\langle \mathcal{J}_z \rangle^2$ upon the electric field intensity for the lower excitonic states with

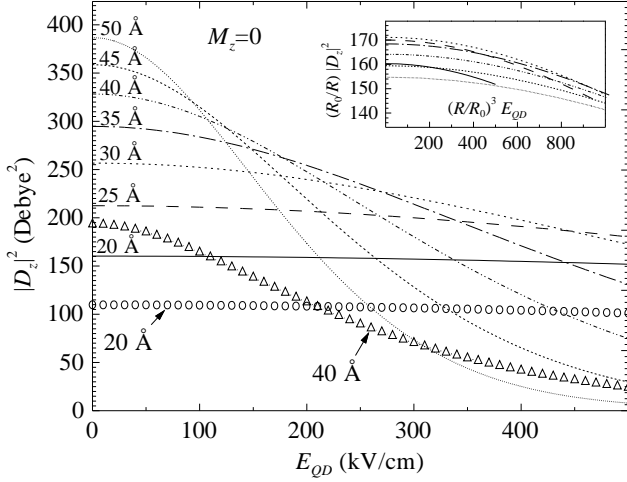


FIG. 5: Allowed dipole matrix elements, $|D_z|^2$, of the lower excitonic states II as function of the applied electric field for CdSe nanocrystals of several radii.

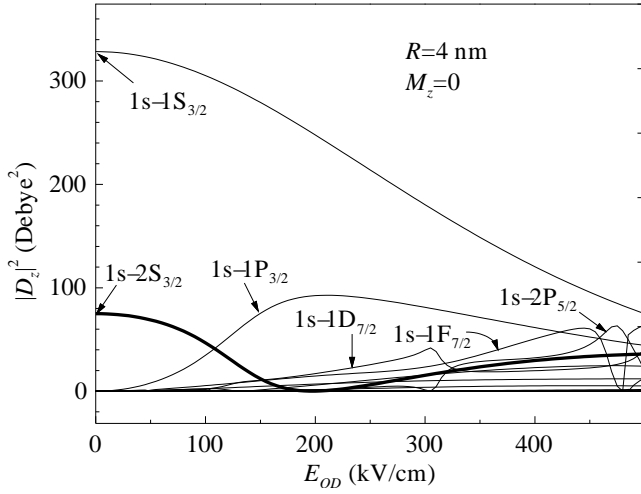


FIG. 6: Dipole matrix element $|D_z|^2$ for a CdSe nanocrystal 4 nm in radius as function of E_{QD} for different excitonic states with angular momentum projection $M_z = 0$.

quantum number $M_z = 0$ for CdSe nanocrystals of several radii. In the inset we present the same results shown in the figure but rescaled according to the laws $(R_0=R)|D_z|^2$ and $(R=R_0)^3 E_{QD}$; where $R_0 = 2$ nm. It can be noticed that $|D_z|^2$ scales almost as R , while the electric field scales as R^3 . The linear dependence of $|D_z|^2$ upon R is a consequence of the Coulomb interaction, i.e. an excitonic effect. For sake of comparison in the Fig. 5 the free electron-hole calculations of $|D_z|^2$ are shown by the triangles and circles for dot radii equal to 2 nm and 4 nm, respectively. As can be seen in the figure, the exciton effects are large, even for small radius of 2 nm. This means that the usual strong confinement approximation, where the Coulomb interaction is considered as a small perturbation, breaks down for small

CdSe nanocrystals. This effect can be explained due to the finite confinement barrier of the electron allowing the penetration of the exciton wave function in the surrounding medium. Also, Fig. 5 indicates that for small radius the optical dipole is not quenched, while for large radius the reduction in photoluminescence intensity should be significant. For example, for a field of 150 kV/cm the square dipole matrix element decreases approximately by 66% for a QD 50 Å in radius, while for a QD of 20 Å, $|D_z|^2$ is almost a constant for the range of the experimental values of the electric field that can be considered. The explanation of the above considered features lies in the interplay between the confinement and electric energies, i.e. the kinetic energy and the external potential energy depend as R^{-2} and R , respectively. In Fig. 6, the behavior of the oscillator strength $|D_z|^2$ as a function of E_{QD} is shown for several excitonic states with angular momentum projection $M_z = 0$. At $E_{QD} = 0$ the exciton oscillator strength is diagonal and only transitions between electrons and holes with S-symmetry are allowed. The field breaks this selection rule and transitions with different symmetry are allowed, i.e. the electric field couples states with $L, l \neq 0$ and the oscillator strength becomes different from zero for s-P, s-D, ... electron-hole pair transitions. The mixing effect, due to E_{QD} , reduces the overlapping between electron and hole states with S-symmetry, allowing other electron-hole transitions. In Fig. 6, the transition 1s-1S_{3/2} is the strongest one over the full range of electric field intensity. For higher transitions, there are kinks at 300 and 480 kV/cm, which are due to avoided crossings between higher levels, e.g., between 1s-1D_{7/2} and 1s-1F_{5/2} at 300 kV/cm (see Fig. 4). Another interesting feature is the disappearance and the appearance of several transitions as the field is tuned. For example, the dipole of the transition 1s-2S_{3/2}, shown as thick line in Fig. 6, is strong at $E_{QD} = 0$ and disappears at $E_{QD} = 180-220$ kV/cm. The opposite can be argued for the 1s-1D_{7/2} and 1s-1F_{7/2} transitions, for which the dipole matrix elements reach a maximum and at higher field intensities they have practical zero oscillator strength. Furthermore, the transition 1s-2S_{3/2} reappears at higher E_{QD} .

V. DISCUSSION

Our calculation reproduces the magnitude of the Stark shift, which can be as large as 80 meV for internal field intensity of 500 kV/cm in nanocrystals 4 nm in radius. This value agrees well in magnitude with the experimental observations of Ref. 8 if one considers that the maximum of the optical gap indicates the zero of the internal electric field under an applied external potential. The presence of an internal electric field and other features of single dot luminescence are currently attributed to trapped charges near the surface of the nanocrystal.^{8,36,37,38,39} Large dipole moments for the ground state and the LUMO in intrinsic CdSe

nanocrystals were predicted by a set of pseudopotential calculations,⁴⁰ which can also account for the linear Stark shift in single dots. This intrinsic dipole moment is associated with the lack of inversion symmetry in wurtzite lattice and depends upon dot structural details and the dielectric response of the surrounding medium. The same calculation also reports null dipole moments for CdSe dots with zinc-blende structure, thus supporting our theoretical model.

Our results are qualitatively similar to those of Fu⁴¹ for InP QD, with the exception of non zero dipole moment at zero field. Due to the inversion symmetry of our hole Hamiltonian (2), the hole eigenstates have definite parity and zero dipole moment. A finite dipole moment, caused by the lack of inversion symmetry in the zinc-blende structure, can be obtained if a linear term in k is included in the $k \cdot p$ Hamiltonian (2). This effect is tiny in bulk semiconductors and is usually neglected. In nanocrystals the dipole may arise from mixing of the hole states $1S_{3=2}$ and $1P_{3=2}$. The amount of mixing depends upon the ratio of the k linear term matrix element ($\propto 1/R$) to the energy separation of the level ($\propto 1/R^2$). Hence, the dipole should be small for small nanocrystals with zinc-blende lattice. For large nanocrystals the bulk regime is approached and the linear terms are again negligible. Although it is not possible to predict with certainty the dipole behavior for intermediate dot sizes, its absolute value should not grow. This is consistent with the calculations of Refs. 40 and 41.

An anomalous field dependence of emission lines of self-assembled quantum dots (SAQD) has been observed through micro-photoluminescence measurements,⁵ where certain transitions lines of the luminescence spectrum disappear and reappear as the electric field is tuned. This feature could not be accounted for using a 1D model of the quantum confinement.⁵ The dipole matrix element of the state $1s-2S_{3=2}$ (Fig. 6) displays that behavior, which could be a property of the 3D confinement. However, a detailed calculation with the SAQD symmetry is needed to test this hypothesis.

Let us consider two simple configurations for photoluminescence experiments. First, the emitted light, with wave vector \mathbf{k} , is recorded along the E_{QD} direction and its polarization vector \mathbf{e}_1 is parallel to $\hat{\mathbf{e}}_x$; (that is, $\mathbf{e}_1 \parallel \hat{\mathbf{e}}_x \perp E_{QD}$). In this case the dipole element $D_x = \hat{\mathbf{e}}_x \cdot \mathbf{D}_{eg}$ is not zero and, according to Table I, the states with $M_z = \pm 1$ of the lowest excitonic level are optically active. Photoluminescence spectra should provide the Stark splitting presented in Fig. 2. Second, the emitted light is observed perpendicular to the field ($\mathbf{k} \perp E_{QD}$). Here, we have two choices for the light polarization, (i) $\mathbf{e}_1 \parallel E_{QD}$ or (ii) $\mathbf{e}_1 \perp E_{QD}$. In the case (i), $\mathbf{e}_1 \parallel \hat{\mathbf{e}}_z \perp \hat{\mathbf{e}}_{M_z=0}$ and the emitted light corresponds to the excitonic state II and the photoluminescence spectrum presents only one peak. In the configuration (ii), both excitonic states I and II are activated and the Stark splitting of Fig. 2 appears. The case (ii) is illustrated in Fig. 7 for the absorption spectra of a single QD at

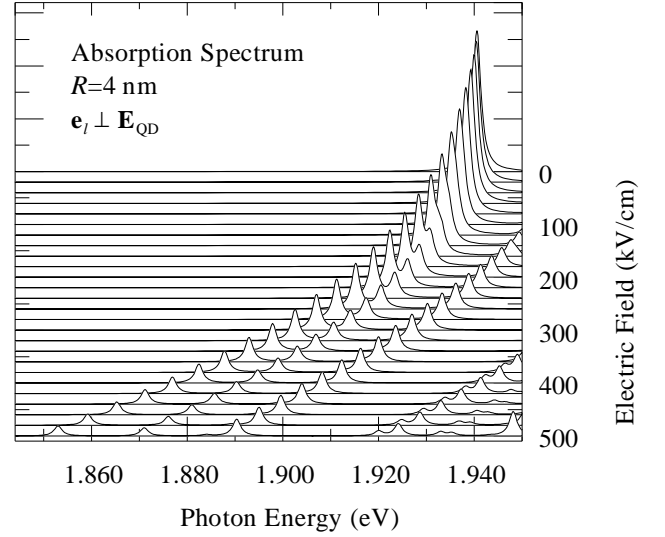


FIG. 7: Absorption spectra for a CdSe nanocrystal at different electric field intensities. The light wave vector and its polarization \mathbf{e}_1 are perpendicular to the electric field.

different electric fields. In the figure, the quenching of the absorption lines and the split of the $1s-1S_{3=2}$ exciton peak as the electric field increases are clearly observed.

The above picture is slightly modified by the cubic anisotropy. At zero electric field, the 8-fold degenerate $1s-1S_{3=2}$ excitons belong to the representations D_1 ($M = 1$) and D_2 ($M = 2$) of group $O(3)$. It is remarkable that the Coulomb interaction does not remove the degeneracy of D_1 and D_2 , and neither does it for higher levels. According to the compatibility tables for groups $O(3)$ and T_d ,³² $D_1 = \psi_5$ and $D_2 = \psi_3 + \psi_4$. Hence, the $M = 1$ triplet is not splitted. As only ψ_5 is dipole allowed, the selection rule $M = 1$ remains valid for the ground exciton state. Only exciton states $ns-N S_{3=2}$ belong to D_1 and are dipole allowed in the spherical approximation. The rest of the states, except $ns-N P_{1=2}$, split in different levels that include ψ_5 and should produce weak lines in the optical spectra. For non-zero electric field, the $O(3)$ symmetry is reduced to C_{1v} , and the irreducible representations correspond to the different values of M_z . The effect of the cubic terms depend upon the orientation of the crystal axes relative to the electric field. If E_{QD} is parallel to a 3-order axis, the symmetry is reduced to C_{3v} . Hence, the excitons with $M_z = 0$ and $M_z = \pm 1$ belong to the ψ_1 and ψ_3 irreducible representations of C_{3v} , respectively, and are not modified by the symmetry reduction. Excitons with higher M_z can split and give rise to weak optical transitions. If the electric field is not oriented along a 3-order axis, all the degeneracies are removed and additional transitions should appear. However, as the cubic anisotropy is induced fundamentally through the hole states, the splittings and intensities of the extra lines should be extremely small.

The fine structure that we have revealed can be modified

- Electronic address: eariel99@yahoo.com ; Present address: Departamento de Física, Universidad de Santiago de Chile, Casilla 307, Santiago 2, Chile.
- ¹ E. E. Mendez, G. Bastard, L. L. Chang, L. Esaki, H. Morkoc, and R. Fischer, *Phys. Rev. B* 26, 7101 (1982).
 - ² D. A. B. Miller, D. S. Chemla, T. C. Damen, A. C. Gossard, W. Wiegmann, T. H. Wood, and C. A. Burrus, *Phys. Rev. Lett.* 53, 2173 (1984).
 - ³ C. M. A. Kapteyn, F. Heinrichsdorff, O. Stier, R. Heitz, M. Grundmann, N. D. Zakharov, D. Binberg, and P. Wemer, *Phys. Rev. B* 60, 14265 (1999).
 - ⁴ D. A. B. Miller, D. S. Chemla, and S. Schmitt-Rink, *Appl. Phys. Lett.* 52, 2154 (1988).
 - ⁵ S. Raymond, J. P. Reynolds, J. L. Merz, S. Fafard, Y. Feng, and S. Charbonneau, *Phys. Rev. B* 58, R13415 (1998).
 - ⁶ P. W. Fry, I. E. Itskevich, D. J. Mowbray, M. S. Skolnick, J. J. Finley, J. A. Barker, E. P. O'Reilly, L. R. Wilson, I. A. Larkin, P. A. Maksym, et al., *Phys. Rev. Lett.* 84, 733 (2000).
 - ⁷ A. D. Yoo, *Adv. Phys.* 50, 1 (2001).
 - ⁸ S. A. Empedocles and M. G. Bawendi, *Science* 278, 2114 (1997).
 - ⁹ S. A. Banton, M. A. Hines, and P. Guyot-Sionnest, *Appl. Phys. Lett.* 69, 3905 (1996).
 - ¹⁰ L. Vina, R. T. Collins, E. E. Mendez, and W. I. Wang, *Phys. Rev. Lett.* 58, 832 (1987).
 - ¹¹ G. E. W. Bauer and T. Ando, *Phys. Rev. Lett.* 59, 601 (1987).
 - ¹² G. E. W. Bauer and T. Ando, *Phys. Rev. B* 38, 6015 (1988).
 - ¹³ L. T. Canham, *Appl. Phys. Lett.* 57, 1046 (1990).
 - ¹⁴ M. V. Wolkin, J. Jome, P. M. Fauchet, G. Allan, and C. Delerue, *Phys. Rev. Lett.* 82, 197 (1999).
 - ¹⁵ A. L. Efros, M. Rosen, M. Kuno, M. Nimai, D. J. Norris, and M. Bawendi, *Phys. Rev. B* 54, 4843 (1996).
 - ¹⁶ E. Casado and C. Trallero-Giner, *Phys. Status Solidi B* 196, 335 (1996).
 - ¹⁷ G. W. Wen, J. Y. Lin, H. X. Jiang, and Z. Chen, *Phys. Rev. B* 52, 5913 (1995).
 - ¹⁸ A. Baldereschi and N. O. Lipari, *Phys. Rev. B* 8, 2697 (1973).
 - ¹⁹ K. Chang and J.-B. Xia, *J. Appl. Phys.* 84, 1454 (1998).
 - ²⁰ E. Mendez-Proupin, *J. Appl. Phys.* (2003), submitted.
 - ²¹ E. Mendez, C. Trallero-Giner, and M. Cardona, *Phys. Status Solidi B* 199, 81 (1997).
 - ²² J. D. Jackson, *Classical Electrodynamics* (Wiley, New York, 1962).
 - ²³ L. R. Aggarwal, in *Modulation Techniques*, edited by P. K. Willardson and A. C. Beer (Academic, New York, 1974), vol. 9 of *Semiconductors and Semimetals*, p. 151.
 - ²⁴ D. M. Brink and G. R. Satchler, *Angular Momentum* (Clarendon Press, Oxford, 1968).
 - ²⁵ U. E. H. Laheld and G. T. Einevoll, *Phys. Rev. B* 55, 5184 (1997).
 - ²⁶ O. Madelung, ed., *Landolt-Bornstein Numerical Data and Functional Relationships in Science and Technology*, vol. III/22 (Springer, Berlin, 1986).
 - ²⁷ C. Hermann and C. Weisbuch, *Phys. Rev. B* 15, 823 (1977).
 - ²⁸ E. Mendez-Proupin, C. Trallero-Giner, and A. Garcia-Cristobal, *Phys. Rev. B* 60, 5513 (1999).
 - ²⁹ J.-B. Xia, *Phys. Rev. B* 40, 8500 (1989).
 - ³⁰ A. L. Efros, *Phys. Rev. B* 46, 7448 (1992).
 - ³¹ A. Baldereschi and N. O. Lipari, *Phys. Rev. B* 9, 1525 (1974).
 - ³² G. F. Koster, J. O. Dimmock, R. G. Wheeler, and H. Statz, *Properties of the thirty-two point groups* (MIT Press, Cambridge, Massachusetts, 1963).
 - ³³ E. Mendez-Proupin and N. Cabo-Bisset, *Phys. Rev. B* 66, 085317 (2002).
 - ³⁴ J. A. Kash, E. E. Mendez, and H. Morkoc, *Appl. Phys. Lett.* 46, 173 (1985).
 - ³⁵ R. C. Miller and A. C. Gossard, *Appl. Phys. Lett.* 43, 954 (1983).
 - ³⁶ L. Wang, *J. Phys. Chem. B* 105, 2360 (2001).
 - ³⁷ A. Eychmuller, *J. Phys. Chem. B* 104, 6514 (2000).
 - ³⁸ J. Tittel, W. Gohde, F. Koberling, T. Basche, A. Komowski, H. Weller, and A. Eychmuller, *J. Phys. Chem. B* 101, 3013 (1997).
 - ³⁹ M. Shim, C. Wang, and P. Guyot-Sionnest, *J. Phys. Chem. B* 105, 2369 (2001).
 - ⁴⁰ E. Rabani, B. Hetenyi, B. J. Berne, and L. E. Brus, *J. Chem. Phys.* 110, 5355 (1999).
 - ⁴¹ H. Fu, *Phys. Rev. B* 65, 045320 (2002).
 - ⁴² V. M. Fomin, V. N. Gladilin, J. T. Devreese, E. P. Pokatilov, S. N. Balaban, and S. N. Klimin, *Phys. Rev. B* 57, 2415 (1998).
 - ⁴³ L. Banyai, P. Gilliot, Y. Z. Hu, and S. W. Koch, *Phys. Rev. B* 45, 14136 (1992).